

Cosmology with quasars: predictions for eROSITA from a quasar Hubble diagram

Lusso Elisabeta^{1,*}

¹ *Dipartimento di Fisica e Astronomia, Università di Firenze, via G. Sansone 1, 50019 Sesto Fiorentino, Firenze, Italy*

² *INAF – Osservatorio Astrofisico di Arcetri, Largo Enrico Fermi 5, 50125 Firenze, Italy*

Correspondence*:
Corresponding Author
elisabeta.lusso@unifi.it

ABSTRACT

The effort for understanding the matter and energy content of the Universe and its evolution relies on different probes, such as cosmic background radiation, cluster lensing, supernovae. Yet, we are still far from grasping what dark matter is made of, and what the physical origin of dark energy is. Our group has developed a technique that makes use of the observed non-linear relation between the ultraviolet and the X-ray luminosity in quasars to provide an independent measurement of their distances, thus turning quasars into *standardizable* candles. This technique, at present, it is mostly based upon quasar samples with data from public catalogues both in the X-rays and in the optical/ultraviolet and extends the Hubble diagram of supernovae to a redshift range still poorly explored ($z > 2$). From the X-ray perspective, we are now on the eve of a major change, as the upcoming mission eROSITA is going to provide us with up to ~ 3 millions of active galactic nuclei across the entire sky. Here we present predictions for constraining cosmological parameters such as the amount of dark matter (Ω_m), dark energy (Ω_Λ) and the evolution of the equation of state of dark energy (w) through the Hubble diagram of quasars, based on the 4-year eROSITA all-sky survey. Our simulations show that the eROSITA quasars, complemented by redshift and broad-band photometric information, will supply the largest quasar sample at $z < 2$, but with very few objects available for cosmology at higher redshifts that survives the cut for the *Malmquist bias*, as eROSITA will sample the brighter end of the X-ray luminosity function. The power of the quasar Hubble diagram for precision cosmology lies in the high-redshift regime, where quasars can be observed up to redshift ~ 7.5 , essential to discriminate amongst different model extrapolations. Therefore, to be competitive for cosmology, the eROSITA quasar Hubble diagram must be complemented with the already available quasar samples and dedicated (deep) large programmes at redshift $z > 3$.

Keywords: active galactic nuclei, quasar, observational cosmology, dark energy, surveys

1 INTRODUCTION

The driving forces behind the present era of precision cosmology have been the detection of anisotropies in the cosmic microwave background (CMB; e.g. Smoot et al. 1) and the discovery of the accelerated expansion of the Universe, based on the Hubble diagram (i.e. the distance modulus versus redshift relation) of Type Ia supernovae (SNe Ia), the standard candles *par excellence* [e.g. 2, 3]. The currently accepted parameterization of our Universe is based on the so-called Λ Cold Dark Matter (Λ CDM) model, hinging upon the existence of cold dark matter and on the cosmological constant (Λ). The nucleosynthesis of

primordial elements, the large-scale galaxy distribution, and gravitational lensing are some of the usual probes into the nature of dark matter, and into how this interacts with visible (baryonic) matter. Yet, we are still far from grasping what the real constituents of this invisible cosmic ingredient are. Moreover, both the physical origin and the properties of dark energy are still unknown, as the interpretation of Λ is plagued by the extreme degree of fine tuning required to obtain the right amount of dark energy observed today. Only the combination of multiple perspectives and of the optimal cosmological probes at different redshifts is the way forward to solve the dark matter and dark energy problems.

In the past years, our group has developed a technique that makes use of the observed non-linear relation between the optical/ultraviolet and the X-ray luminosity in quasars [e.g. 4, 5, 6, 7]. In contrast to previous ideas of high stochasticity, this relation can be employed to standardize the emission of quasars [8, 9]. The methodology is complementary to the traditional resort to Type Ia SNe to estimate the cosmological parameters, yet it extends the Hubble diagram to a redshift range currently inaccessible to supernovae ($z = 2 - 6$). The tightness of the UV-to-X-ray relation across both a wide redshift (up to $z \simeq 5 - 6$) and luminosity range (see Lusso and Risaliti 7) must be the manifestation of a universal physical mechanism that governs the disc-corona synergy in the quasar engines, yet the details of the physical process originating this relation is still unknown [e.g. 10].

The main result of our work is that the distance modulus/redshift relation of quasars at $z < 1.4$ is in agreement with that of supernovae and with the concordance model [8, 9]. Yet, a deviation from the Λ CDM model emerges at higher redshift, with a statistical significance of 4σ . If we consider an evolution of the dark energy equation of state in form $w(z) = w_0 + w_a \times z/(1 + z)$, the data suggest that the dark energy density is increasing with time [9, 11].

In order to build a quasar sample that can be utilised for cosmological purposes, both X-ray and optical/UV data are required to cover the rest-frame 2 keV and the 2500 Å. At the time of writing, the most extended spectroscopic coverage in the optical/UV is provided by the *Sloan Digital Sky Survey* [12], which supplies more than $\sim 500,000$ quasars with spectroscopic redshift up to $z \sim 7$. This sample needs to be cross-matched with the current X-ray catalogues, namely the *Chandra* CXC2.0¹ [13] and the 3XMM Data Release 8² [14], which contain *all the X-ray sources detected by the XMM-Newton and Chandra observatories that are publicly available in the archives*. The number of quasars with a detection in both the UV and X-rays ranges from about a few thousands to $\sim 13,000$, respectively. Once our filtering criteria are applied to select blue quasars with low levels of UV reddening and X-ray absorption and the Malmquist bias is corrected (the interested reader should refer to Risaliti and Lusso 8, Lusso and Risaliti 7, Bisogni et al. 15, Risaliti and Lusso 11 for details on the sample selection), the final samples drastically reduce to less than 2,000 objects (~ 1000 in the case of SDSS-CXC2.0, Bisogni et al. in preparation). Our leverage in building extended quasar samples for cosmology is thus entirely based upon archival data of pointed X-ray observations, which cover a very limited portion of the sky compared to SDSS, i.e. roughly 1000 deg^2 for both 3XMM-DR8 and CXC2.0 compared to $>14,000 \text{ deg}^2$ for SDSS.

We are now on the eve of the next major revolution in the field of X-ray astrophysics. The *extended Roentgen Survey with an Imaging Telescope Array* (eROSITA, Predehl 16, Merloni et al. 17) is the flagship instrument of the Russian *Spektrum-Roentgen-Gamma* (SRG) mission, and it will represent the most powerful and versatile X-ray observatory of the next decade. In the first 4 years of scientific operations, eROSITA will perform 8 deep scans of the entire sky, one every six months. When completed, the survey

¹ <http://cxc.cfa.harvard.edu/csc2/>

² <http://xmmssc.irap.omp.eu/Catalogue/3XMM-DR8/3XMM-DR8.html>

will be ~ 20 times deeper than ROSAT at 0.5–2 keV, and it will provide the very first sensitive imaging of the whole sky in the hard band (2–10 keV). eROSITA will bring an improvement of over two orders of magnitude in the number of sources shining close to or above the break in the X-ray luminosity function (i.e. Fig. 5.2.2 in Merloni et al. 17). eROSITA's sky will be dominated by the active galactic nuclei (AGN) population, with ~ 3 million AGN expected by the end of the nominal 4-year all-sky survey at the sensitivity of $F_{0.5-2\text{ keV}} \simeq 10^{-14} \text{ erg s}^{-1} \text{ cm}^{-2}$ and with a median redshift of $z \sim 1$.

In this work we discuss the potential of the 4-year eROSITA all-sky survey for constraining cosmological parameters such as Ω_m , Ω_Λ and w , through the Hubble diagram of quasars.

2 THE SIMULATED EROSITA QUASAR SAMPLE

The SDSS-DR14 quasar catalogue contains 526,356 objects with $0.008 < z < 6.968$. We first selected a clean quasar sample in the optical/UV based on the selection criteria discussed in depth in our previous works [7, 8, 11]. The main goal of this first step is to obtain the *intrinsic* flux at the rest-frame 2500 Å. We excluded all quasars flagged as broad absorption line (BAL, BI_CIV=0) and selected only the sources with a detection in all SDSS photometric bands, leading to a preliminary sample of 503,746 quasars. The SDSS-DR14 quasar catalogue also provides us with multi-wavelength information from several surveys, from the radio (FIRST survey) to the UV (GALEX survey; see section 7 in Pâris et al. 12). Thanks to this extended multi-band coverage, we built the spectral energy distributions (SEDs) that are then employed to compute the slope Γ_1 of a $\log(\nu) - \log(\nu F_\nu)$ power law in the 0.3–1 μm (rest frame) range, and the analogous slope Γ_2 in the 0.3–0.145 μm range (rest frame). We assumed a standard SMC extinction law (Prevot et al. 18, appropriate for unobscured quasars, Hopkins et al. 19, Salvato et al. 20) to estimate the $\Gamma_1 - \Gamma_2$ correlation as a function of extinction (parametrized by $E(B-V)$). The $\Gamma_1 - \Gamma_2$ value that corresponds to zero extinction ($E(B-V)=0$) is derived from the standard quasar SED of Richards et al. [21, i.e. $\Gamma_1 = 0.82$, $\Gamma_2 = 0.40$]. We then selected all objects within a circle centered at $E(B-V)=0$ with a radius of 0.8 (i.e. $E(B-V)<0.1$). From the SED we also calculated the flux at the rest-frame 2500 Å (F_{2500}) and the one at 6 cm from the FIRST flux using a slope of -0.8 , and we further excluded all the objects with $F_{6\text{ cm}}/F_{2500} > 10$. We also excluded all quasars in the sample defined as radio loud in the MIXR catalogue [22] within a matching radius of 2 arcsec. This leads to a final clean sample in the UV of 291,944 quasars, within a redshift interval $0.061 < z < 5.25$ ($\langle z \rangle \simeq 1.8$).

Since eROSITA is expected to survey the entire X-ray sky down to a flux that well matches the SDSS quasar optical magnitudes, we forecast that almost all SDSS quasars will be detected by eROSITA [23]. We thus simulated an X-ray flux measurement for each object as follows.

We assumed the observed linear $\log F_{2\text{ keV}} - \log F_{2500}$ relation, with a slope $\alpha = 0.6$, a flat Λ CDM cosmology with $H_0 = 70 \text{ km s}^{-1} \text{ Mpc}^{-1}$, $\Omega_m = 0.3$ and $\Omega_\Lambda = 1 - \Omega_m$, and a dispersion in the $F_{2\text{ keV}} - F_{2500}$ relation on the order of 0.1 dex. These values have been chosen to be representative of the mainstream models, although we know that the constraints on the cosmological parameters from observations in the local and in the early Universe are somewhat different (see Section 4.1). We started from fluxes as they are cosmology independent, and we have demonstrated in our previous works that the $\log F_{2\text{ keV}} - \log F_{2500}$ relation in narrow redshift bins displays the same slope (i.e. $\gamma \simeq 0.6$) across a wide redshift range (see Figure 8 in Risaliti and Lusso 11 supplementary material). Moreover, the main aim of our simulations is to quantify the expected uncertainties on the cosmological parameters rather than focus on the absolute values per se. As such, we defer possible extensions of these simulations to non standard cosmological values and to a possible evolution of these parameters with redshift to future works.

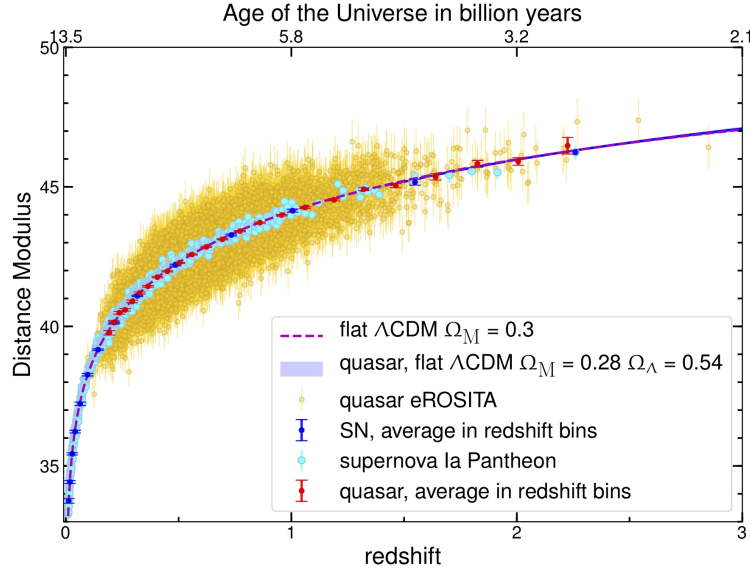


Figure 1. Hubble diagram of eROSITA quasars ($\sim 11,000$, yellow points) and SNe Ia (*Pantheon*, cyan points) with 1σ uncertainties. Red points are the mean (also with 1σ uncertainties) of the distance modulus in narrow redshift bins for quasars only (shown for visualisation purposes). The dashed magenta line shows a flat Λ CDM model fit with $\Omega_m = 0.3$. The blue line is the best MCMC fit of the eROSITA quasars (with uncertainties) only for a Λ CDM cosmology where Ω_m and Ω_Λ are left free to vary (§ 3).

As the eROSITA survey is flux limited, we also need to take into account the *Malmquist bias* (also known as the Eddington bias), which is a redshift dependent correction. We conservatively assumed an observed flux limit in the soft X-ray band of $3 \times 10^{-14} \text{ erg s}^{-1} \text{ cm}^{-2}$, which will be reached after the first year of operations, and considered all the sources with an expected monochromatic flux at 2 keV that corresponds to about twice the value above, i.e. $5 \times 10^{-32} \text{ erg s}^{-1} \text{ cm}^{-2} \text{ Hz}^{-1}$, assuming a photon index of 1.9. This selection leaves very few sources at redshift higher than 2. We obtain a final sample of $\sim 11,000$ quasars in the redshift range 0.061–2.850, with a mean redshift $\langle z \rangle \simeq 0.64$, consistent with the predicted statistical properties based on the best available redshift-dependent AGN X-ray luminosity function [24].

3 RESULTS

The distance modulus-redshift relation of the eROSITA quasars is presented in Figure 1 with 1σ uncertainties. The error bars on the distance modulus values for the quasar sample are estimated by propagating the uncertainties on the slope γ , $F_{2\text{keV}}$ and F_{2500} . We assumed typical uncertainties on the slope and $F_{2\text{keV}}$ of 0.02 and 20%, respectively. Uncertainties on F_{2500} are computed by propagating the magnitude uncertainties from the SEDs we compiled for each SDSS quasar in the catalogue (see § 2 in Risaliti and Lusso 11 supplementary material). The red points are the mean (also with 1σ uncertainties) of the distance modulus in narrow redshift bins for quasars (shown for visualisation purposes). Here we also show the SNe Ia sample from the *Pantheon* survey consisting of 1048 objects ranging from $0.01 < z < 2.26$ [25]. The dashed magenta line shows the input flat Λ CDM cosmology with $\Omega_m = 0.3$ and $\Omega_\Lambda = 0.7$.

We then fitted to this sample a Λ CDM model where Ω_m and Ω_Λ are left free to vary, and a model with a dark energy equation of state parameter w (assuming a flat Universe, w CDM). The results are shown in Figure 2, whilst a summary of the predictions on the cosmographic parameters from the analysis of the eROSITA quasar Hubble diagram is presented in Table 1. The confidence contours are at 68% and 95%

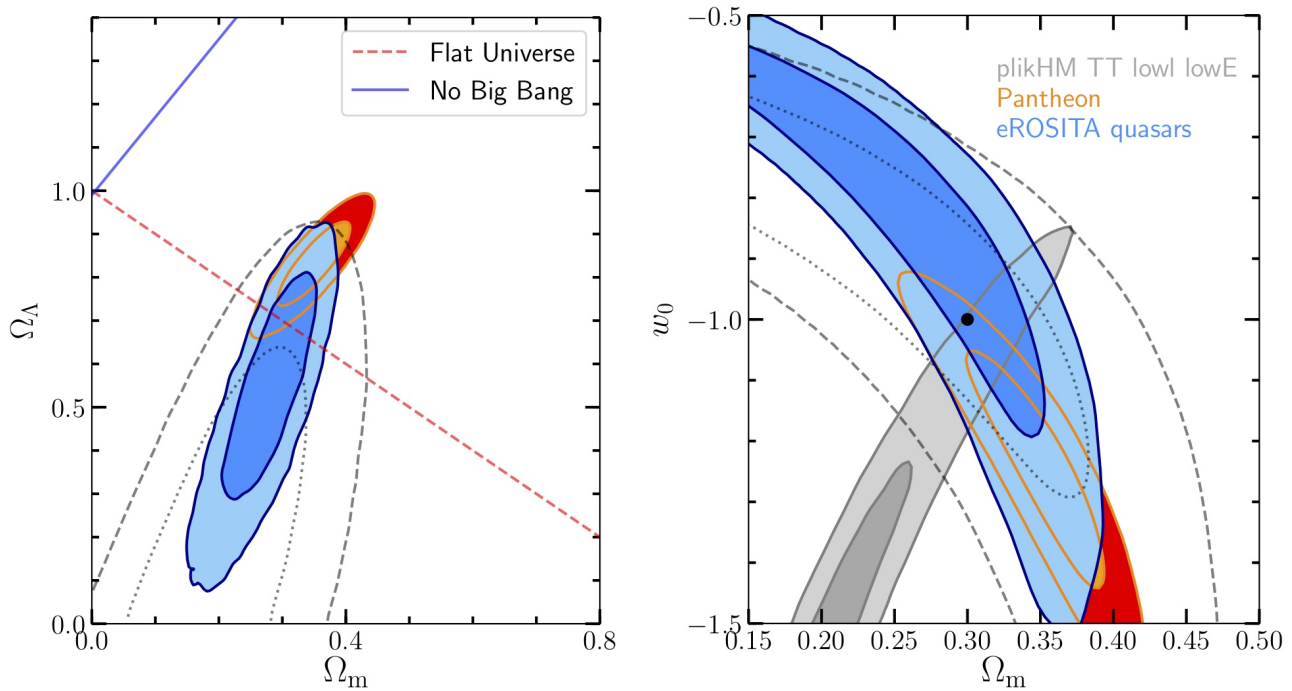


Figure 2. *Left panel:* Confidence contours at 68% and 95% levels for the Ω_m and Ω_Λ cosmological parameters in the Λ CDM model, where both Ω_m and Ω_Λ are free to vary. All the plotted uncertainties are statistical. Orange/red contours: *Pantheon*. Blue/cyan: eROSITA simulated sample. *Right panel:* Confidence contours at 68% and 95% levels for the Ω_m and w cosmological parameters in the w CDM model. All the plotted uncertainties are statistical. Orange/red contours: *Pantheon*. Filled dark/light gray: *Planck* constraints from a Plik TT+lowl+lowE likelihood. Blue/cyan: eROSITA simulated sample. The dashed/dotted contours represent the constraints on the cosmological parameters of a mock eROSITA quasar sample of $\sim 17,000$ quasars assuming a dispersion in the $L_{2\text{keV}} - L_{2500}$ relation of 0.2 dex.

levels and all the plotted uncertainties are statistical, computed from the marginalized posterior probability distributions. All the simulations have been performed through a standard fully Bayesian procedure by making use of the affine invariant Monte Carlo Markov Chain ensemble sampler [26]. We adopted uniform priors on the cosmological parameters with $0 < \Omega_m < 1.2$ and $0 < \Omega_\Lambda < 1.5$ for the Λ CDM model, whilst we used $0 < \Omega_m < 1.2$ and $-3 < w < 1$ for w CDM. The adopted likelihood also contains an intrinsic dispersion (δ) as a free parameter (see Risaliti and Lusso 11 for details). An additional free parameter is the cross-calibration (β') between supernovae Ia and quasars. Overall we have four free parameters for both the Λ CDM (i.e. Ω_m , Ω_Λ , β' and δ) and the flat w CDM (i.e. Ω_m , w_0 , β' and δ).

Our method governs the shape of the Hubble diagram, whilst to determine the absolute value of the distances we need an external calibrator to build the distance ladder (like Cepheids are for supernovae Ia).

As a consequence of the marginalization over the β' , our technique does not provide any direct constraint on the Hubble parameter, H_0 . In the simulations, the value of H_0 used for the calibration with the supernovae Ia is thus assumed and then marginalized over β' . Considering a different value of H_0 would just modify the final cross-calibration with no change on the values of the best fit cosmological parameters and confidence intervals.

Model	Ω_m	Ω_Λ	w_0	w_a
Λ CDM	0.28 ± 0.05	$0.54^{+0.17}_{-0.19}$	—	—
w CDM	$0.26^{+0.07}_{-0.11}$	—	$-0.81^{+0.22}_{-0.28}$	—

Table 1. Prediction on the cosmographic parameters from the analysis of the eROSITA quasar Hubble diagram.

4 DISCUSSION

The precision on Ω_m that can be achieved with the eROSITA quasars only is similar to that obtained today by supernovae Ia in the case Ω_m and Ω_Λ are fitted simultaneously (i.e. $\Omega_m = 0.35 \pm 0.04$, see Table 8 in Scolnic et al. 25). The current accuracy on Ω_Λ from supernovae Ia is $\sim 8\%$, whilst the precision on Ω_Λ from the simulated quasar Hubble diagram is on the order of $\sim 30\%$. This is due to the much higher dispersion of the data in the quasar Hubble diagram with respect to *Pantheon* in the common redshift range. We also note that the assumed dispersion on the $L_{2\text{keV}} - L_{2500}$ relation is rather optimistic. In fact, we can obtain a dispersion of $\sim 0.12 - 0.15$ dex only when we consider pointed X-ray observations (see the Supplementary Material in Risaliti and Lusso [11]), whilst the dispersion in the $L_{2\text{keV}} - L_{2500}$ relation that we can achieve at present is $0.2 - 0.24$ dex. We also considered another mock quasar sample where we assume a dispersion of 0.2 dex, having similar statistics and redshift distribution to the one in Figure 1. The accuracy on Ω_m and Ω_Λ decreases to $\sim 30\%$ and $\sim 40\%$, respectively. The precision on Ω_m is more affected by the increased dispersion in the $L_{2\text{keV}} - L_{2500}$ relation than the one on Ω_Λ . This is somewhat expected given the redshift distribution of the mock sample (see also Figure 5 in Kolodzig et al. 24 for the statistical quasar sample predictions). The range of accuracy on w for the best-case scenario and the more realistic one is shown in Figure 2 for a w CDM.

From our simulations one can conclude that, with the eROSITA quasars alone and the current observed dispersion in the $L_{2\text{keV}} - L_{2500}$ relation, it will be challenging to provide stringent constraints on the cosmological parameters. Nonetheless, the simulated quasar sample does not include the hundreds of quasars at redshift $z > 2.5$ that are already available from the public archives, which would not only improve the precision of the determination of both Ω_m and Ω_Λ , but will allow us to test with greater precision a possible evolution of the equation of state of dark energy with redshift $w(z)$. In fact, the parameter Ω_m is partly degenerate with w_a in models with an evolving equation of state of the dark energy, w_z CDM.

Even with a dispersion on the $L_{2\text{keV}} - L_{2500}$ relation that matches the current ones (see Supplementary Fig. 6 in Risaliti and Lusso 11), thanks to the much greater statistics at redshift lower than 2 offered by eROSITA, we will sample the *knee* of the Hubble diagram with several thousands of sources. The eROSITA sample combined to the high redshift quasars (in particular $z > 3$) from the archives will allow us to test models where the dark energy equation of state w is allowed to evolve with redshift.

4.1 On the tension of the Hubble parameter.

It is clear from the left panel of Figure 2 that CMB data alone do not constrain the equation of state of dark energy, w , due to strong geometrical model degeneracies. Indeed, *Planck* data on their own (i.e. CMB+lensing) can only assess the equation of state with $\sim 30\%$ uncertainty: $w = -1.57^{+0.50}_{-0.40}$, whilst this measure becomes $w = -1.04 \pm 0.1$ by considering a combination of *Planck* with Baryon Acoustic Oscillation (BAO, Planck Collaboration et al. 27, *Planck* collaboration). This value is consistent with the expected one for a cosmological constant in the standard Λ CDM model, but the comparison between the concordance cosmological parameters obtained from the different probes brings out some tensions. For

example, the most recent results from *Planck* assuming the standard Λ CDM cosmology are in tension at the 4.4σ level with the direct measurement of the Hubble parameter (H_0 , which measures the current expansion rate of the Universe) from Cepheids plus supernovae Ia [28], and at about 2.5σ with the matter density estimates from supernovae Ia (e.g. Rest et al. 29) and with the $\text{Ly}\alpha$ BAO measurements (e.g. Delubac et al. 30, Font-Ribera et al. 31). Recently, results on H_0 (assuming a standard flat Λ CDM cosmology) from 6 multiple-imaged quasar systems through strong gravitational lensing have confirmed this tension at more than 5σ level with respect to *Planck* (H0LiCOW collaboration; Wong et al. 32). Whilst the reason for these tensions can be partially alleviated by accounting for the systematics in the different data sets (e.g. dependence of the supernovae Ia luminosity on age, Kang et al. 33), most of the discrepancy still remains unclear. In fact, within the Λ CDM framework, where w is assumed to be constant ($w = -1$) across the cosmic time, there should be no difference between the H_0 value measured locally and the one measured in the early Universe. These discrepancies can in fact be the indication of new physics beyond the standard Λ CDM cosmology.

Our technique does not provide constraints on H_0 since this parameter is degenerate with the absolute cross-calibration of the Hubble diagram. Nonetheless, if we could confirm with high accuracy that w indeed evolves with time (see Risaliti and Lusso 11, Lusso et al. 9), this will provide an independent, compelling proof that this tension is real. Reducing the measurement uncertainties on cosmological parameters has become the main goal of current and forthcoming cosmological projects, in order to either corroborate the standard model or find new physics beyond it (see also results from N-body simulations, e.g. Adamek et al. 34). Only the combination of different approaches, supported by an increased data quality and sample statistics, is the way forward to solve the H_0 tension.

FUNDING

We acknowledge financial contribution from the agreement ASI-INAF n.2017-14-H.O.

ACKNOWLEDGMENTS

This work was initiated at the Aspen Center for Physics, which is supported by National Science Foundation grant PHY-1607611.

This research made use of Astropy a community-developed core Python package for Astronomy [35]. This research made use of Matplotlib, a 2D graphics package used for Python [36].

REFERENCES

- [1] Smoot GF, Bennett CL, Kogut A, Wright EL, Aymon J, Boggess NW, et al. Structure in the COBE Differential Microwave Radiometer First-Year Maps. *ApJ* **396** (1992) L1. doi:10.1086/186504.
- [2] Riess AG, Filippenko AV, Challis P, Clocchiatti A, Diercks A, Garnavich PM, et al. Observational Evidence from Supernovae for an Accelerating Universe and a Cosmological Constant. *AJ* **116** (1998) 1009–1038. doi:10.1086/300499.
- [3] Perlmutter S, Aldering G, Goldhaber G, Knop RA, Nugent P, Castro PG, et al. Measurements of Ω and Λ from 42 High-Redshift Supernovae. *ApJ* **517** (1999) 565–586. doi:10.1086/307221.
- [4] Steffen AT, Strateva I, Brandt WN, Alexander DM, Koekemoer AM, Lehmer BD, et al. The X-Ray-to-Optical Properties of Optically Selected Active Galaxies over Wide Luminosity and Redshift Ranges. *AJ* **131** (2006) 2826–2842. doi:10.1086/503627.

- [5] Just DW, Brandt WN, Shemmer O, Steffen AT, Schneider DP, Chartas G, et al. The X-Ray Properties of the Most Luminous Quasars from the Sloan Digital Sky Survey. *ApJ* **665** (2007) 1004–1022. doi:10.1086/519990.
- [6] Lusso E, et al. The X-ray to optical-UV luminosity ratio of X-ray selected type 1 AGN in XMM-COSMOS. *A&A* **512** (2010) A34. doi:10.1051/0004-6361/200913298.
- [7] Lusso E, Risaliti G. The Tight Relation between X-Ray and Ultraviolet Luminosity of Quasars. *ApJ* **819** (2016) 154. doi:10.3847/0004-637X/819/2/154.
- [8] Risaliti G, Lusso E. A Hubble Diagram for Quasars. *ApJ* **815** (2015) 33. doi:10.1088/0004-637X/815/1/33.
- [9] Lusso E, Piedipalumbo E, Risaliti G, Paolillo M, Bisogni S, Nardini E, et al. Tension with the flat Λ CDM model from a high-redshift Hubble diagram of supernovae, quasars, and gamma-ray bursts. *A&A* **628** (2019) L4. doi:10.1051/0004-6361/201936223.
- [10] Lusso E, Risaliti G. Quasars as standard candles. I. The physical relation between disc and coronal emission. *A&A* **602** (2017) A79. doi:10.1051/0004-6361/201630079.
- [11] Risaliti G, Lusso E. Cosmological constraints from the Hubble diagram of quasars at high redshifts. *Nature Astronomy* (2019) 195. doi:10.1038/s41550-018-0657-z.
- [12] Pâris I, Petitjean P, Aubourg É, Myers AD, Streblyanska A, Lyke BW, et al. The Sloan Digital Sky Survey Quasar Catalog: Fourteenth data release. *A&A* **613** (2018) A51. doi:10.1051/0004-6361/201732445.
- [13] Evans IN, Primini FA, Glotfelty KJ, Anderson CS, Bonaventura NR, Chen JC, et al. The Chandra Source Catalog. *ApJS* **189** (2010) 37–82. doi:10.1088/0067-0049/189/1/37.
- [14] Rosen SR, Webb NA, Watson MG, Ballet J, Barret D, Braitto V, et al. The XMM-Newton serendipitous survey. VII. The third XMM-Newton serendipitous source catalogue. *A&A* **590** (2016) A1. doi:10.1051/0004-6361/201526416.
- [15] Bisogni S, Risaliti G, Lusso E. A Hubble Diagram for Quasars. *Frontiers in Astronomy and Space Sciences* **4** (2017) 68. doi:10.3389/fspas.2017.00068.
- [16] Predehl P. eROSITA. *Society of Photo-Optical Instrumentation Engineers (SPIE) Conference Series* (2012), *Society of Photo-Optical Instrumentation Engineers (SPIE) Conference Series*, vol. 8443, 84431R. doi:10.1117/12.925843.
- [17] Merloni A, Predehl P, Becker W, Böhringer H, Boller T, Brunner H, et al. eROSITA Science Book: Mapping the Structure of the Energetic Universe. *arXiv e-prints* (2012) arXiv:1209.3114.
- [18] Prevot ML, Lequeux J, Prevot L, Maurice E, Rocca-Volmerange B. The typical interstellar extinction in the Small Magellanic Cloud. *A&A* **132** (1984) 389–392.
- [19] Hopkins PF, Strauss MA, Hall PB, Richards GT, Cooper AS, Schneider DP, et al. Dust Reddening in Sloan Digital Sky Survey Quasars. *AJ* **128** (2004) 1112–1123. doi:10.1086/423291.
- [20] Salvato M, et al. Photometric Redshift and Classification for the XMM-COSMOS Sources. *ApJ* **690** (2009) 1250–1263. doi:10.1088/0004-637X/690/2/1250.
- [21] Richards GT, Strauss MA, Fan X, Hall PB, Jester S, Schneider DP, et al. The Sloan Digital Sky Survey Quasar Survey: Quasar Luminosity Function from Data Release 3. *AJ* **131** (2006) 2766–2787. doi:10.1086/503559.
- [22] Mingo B, Watson MG, Rosen SR, Hardcastle MJ, Ruiz A, Blain A, et al. The MIXR sample: AGN activity versus star formation across the cross-correlation of WISE, 3XMM, and FIRST/NVSS. *MNRAS* **462** (2016) 2631–2667. doi:10.1093/mnras/stw1826.

- [23] Menzel ML, Merloni A, Georgakakis A, Salvato M, Aubourg E, Brandt WN, et al. A spectroscopic survey of X-ray-selected AGNs in the northern XMM-XXL field. *MNRAS* **457** (2016) 110–132. doi:10.1093/mnras/stv2749.
- [24] Kolodzig A, Gilfanov M, Sunyaev R, Sazonov S, Brusa M. AGN and QSOs in the eROSITA All-Sky Survey. I. Statistical properties. *A&A* **558** (2013) A89. doi:10.1051/0004-6361/201220880.
- [25] Scolnic DM, Jones DO, Rest A, Pan YC, Chornock R, Foley RJ, et al. The Complete Light-curve Sample of Spectroscopically Confirmed SNe Ia from Pan-STARRS1 and Cosmological Constraints from the Combined Pantheon Sample. *ApJ* **859** (2018) 101. doi:10.3847/1538-4357/aab9bb.
- [26] Foreman-Mackey D, Hogg DW, Lang D, Goodman J. emcee: The MCMC Hammer. *PASP* **125** (2013) 306–312. doi:10.1086/670067.
- [27] Planck Collaboration, Aghanim N, Akrami Y, Ashdown M, Aumont J, Baccigalupi C, et al. Planck 2018 results. VI. Cosmological parameters. *arXiv e-prints* (2018) arXiv:1807.06209.
- [28] Riess AG, Casertano S, Yuan W, Macri LM, Scolnic D. Large Magellanic Cloud Cepheid Standards Provide a 1% Foundation for the Determination of the Hubble Constant and Stronger Evidence for Physics beyond Λ CDM. *ApJ* **876** (2019) 85. doi:10.3847/1538-4357/ab1422.
- [29] Rest A, Scolnic D, Foley RJ, Huber ME, Chornock R, Narayan G, et al. Cosmological Constraints from Measurements of Type Ia Supernovae Discovered during the First 1.5 yr of the Pan-STARRS1 Survey. *ApJ* **795** (2014) 44. doi:10.1088/0004-637X/795/1/44.
- [30] Delubac T, Bautista JE, Busca NG, Rich J, Kirkby D, Bailey S, et al. Baryon acoustic oscillations in the Ly α forest of BOSS DR11 quasars. *A&A* **574** (2015) A59. doi:10.1051/0004-6361/201423969.
- [31] Font-Ribera A, Kirkby D, Busca N, Miralda-Escudé J, Ross NP, Slosar A, et al. Quasar-Lyman α forest cross-correlation from BOSS DR11: Baryon Acoustic Oscillations. *JCAP* **2014** (2014) 027. doi:10.1088/1475-7516/2014/05/027.
- [32] Wong KC, Suyu SH, Chen GCF, Rusu CE, Millon M, Sluse D, et al. H0LiCOW XIII. A 2.4% measurement of H_0 from lensed quasars: 5.3 σ tension between early and late-Universe probes. *arXiv e-prints* (2019) arXiv:1907.04869.
- [33] Kang Y, Lee YW, Kim YL, Chung C, Ree CH. Early-type Host Galaxies of Type Ia Supernovae. II. Evidence for Luminosity Evolution in Supernova Cosmology. *ApJ* **889** (2020) 8. doi:10.3847/1538-4357/ab5afc.
- [34] Adamek J, Daverio D, Durrer R, Kunz M. General relativity and cosmic structure formation. *Nature Physics* **12** (2016) 346–349. doi:10.1038/nphys3673.
- [35] Astropy Collaboration, Price-Whelan AM, Sipőcz BM, Günther HM, Lim PL, Crawford SM, et al. The Astropy Project: Building an Open-science Project and Status of the v2.0 Core Package. *AJ* **156** (2018) 123. doi:10.3847/1538-3881/aabc4f.
- [36] Hunter JD. Matplotlib: A 2D Graphics Environment. *Computing in Science and Engineering* **9** (2007) 90–95. doi:10.1109/MCSE.2007.55.